# Resolution requirements in large-eddy simulations of shear flows

By J. S. Baggett, J. Jiménez[1] AND A. G. Kravchenko

## 1. Motivation

Large eddy simulations reproduce faithfully the characteristics of moderately complex turbulent flows (Moin & Jiménez 1993, Moin 1997). This is true even if most of them are, at present, based on variations of the Smagorinsky model, which is known to represent only poorly the subgrid Reynolds stresses (Clark, Ferziger & Reynolds 1979, Bardina, Ferziger & Reynolds 1983). The subgrid stress tensor can be decomposed in isotropic and anisotropic components. The former affects the flow by determining the rate of energy dissipation, but it does not enter directly in the equations for the mean flow. The average value of the latter determines the mean shear stresses and controls directly the mean velocity profiles. In the absence of a mean shear, the rate of energy dissipation fully characterizes isotropic turbulence (Kolmogorov 1941), and it is believed that the dynamic versions of the Smagorinsky model (Germano *et al.* 1991) work by approximating it correctly (Jiménez 1995). It is, on the other hand, clear that a model which does not well represent the stresses must do a poor job on shear flows unless the resolution of the filter is chosen fine enough that the subgrid stresses are negligible.

While it has long been recognized that adequate resolution is crucial for successful large-eddy simulations, there are few systematic studies that delineate the actual requirements. That is the subject of this note. The issue may actually be of secondary importance in free shear flows, although a clear criterion should also be useful there because it will be shown below that the number of 'anisotropic' degrees of freedom in those flows is independent of the Reynolds number. Large-eddy simulations only have to compute explicitly those anisotropic modes since, as discussed in the previous paragraph, the isotropic ones are handled well by the present models. It follows that large-eddy simulations of free shear flows need only resolve a fixed number of degrees of freedom, depending on the geometry but independent of Reynolds number, and that an overestimation of the resolution requirements would at most result in a fixed penalty factor in computer time.

The situation is different for wall-bounded flows, in which the decrease of the integral scales in the neighborhood of the wall results in a number of anisotropic modes which increases with Reynolds number. The resolution requirements for LES depend, as a consequence, also on the Reynolds number and, although not as large as those of direct simulations, are at present the main limitation for the simulation of those flows (Chapman 1979). It is therefore important in those cases to understand the exact requirements and their causes.

1 Also with the School of Aeronautics, U. Politécnica Madrid.

The present note is organized as follows. In §2 we review the experimental evidence on the anisotropy of the small scales and, in particular, on the dependence of the subgrid off-diagonal stresses with the size of the filter. This section also includes information on the equivalent width to be used for this purpose in anisotropic filters. The predicted stresses are compared in §3 to those obtained by a standard dynamic Smagorinsky model, and a criterion is established for the resolution needed to achieve a given error in the mean flow. The number of computational modes required for large-eddy simulations is estimated from these arguments in §4, and guidelines are offered for further work.

## 2. The anisotropy of the subgrid stresses

### *2.1 Spectral information*

Although it is generally accepted that the small scales of turbulent flows are isotropic, quantitative measurements are rare (see Saddoughi & Veeravalli, 1994, for a recent experiment and for a review of older results). From the point of view of LES, what is needed is a characterization of the isotropy of the subgrid Reynolds stress tensor. Consider the spectral energy tensor $\Phi_{ij}$, which is a function of the wavenumber vector $\mathbf{k}$. If it is normalized so that $\int \Phi_{ij}\,\mathrm{d}\mathbf{k} = \overline{u_i u_j}$, the truncated integral

$$\tau_{ij}(k) = \int_{|\mathbf{k}|>k} \Phi_{ij}\,\mathrm{d}\mathbf{k}, \tag{2.1}$$

represents the subgrid stress tensor corresponding to a sharp filter with cut-off $k$. For each $k$ it is then possible to define a stress anisotropy tensor,

$$A_{ij} = \frac{\tau_{ij}}{\tau_{kk}} - \frac{1}{3}\delta_{ij}, \tag{2.2}$$

where repeated indices imply summation, and its $L_2$ norm, normalized as

$$\alpha = (A_{ij}A_{ij}/3)^{1/2}, \tag{2.3}$$

measures the anisotropy of the subgrid stresses. It is proportional to the root mean square deviation of the principal stresses with respect to their mean value, normalized with the subgrid energy. It reaches a maximum value of $\alpha \approx 0.47$ for a completely uni-axial stress and is zero for an isotropic tensor.

In practice this quantity is seldom available, and the one-dimensional spectral tensor $\Theta_{ij}(k_1)$, obtained by integrating $\Phi_{ij}$ over the two remaining wavenumber components, is used as a surrogate. The subgrid stresses are then estimated by

$$\tau_{ij}(k) = \int_k^\infty \Theta_{ij}\,\mathrm{d}k_1, \tag{2.4}$$

which corresponds to applying a one-dimensional sharp filter with cut-off $k_1 = k$ along the streamwise direction.

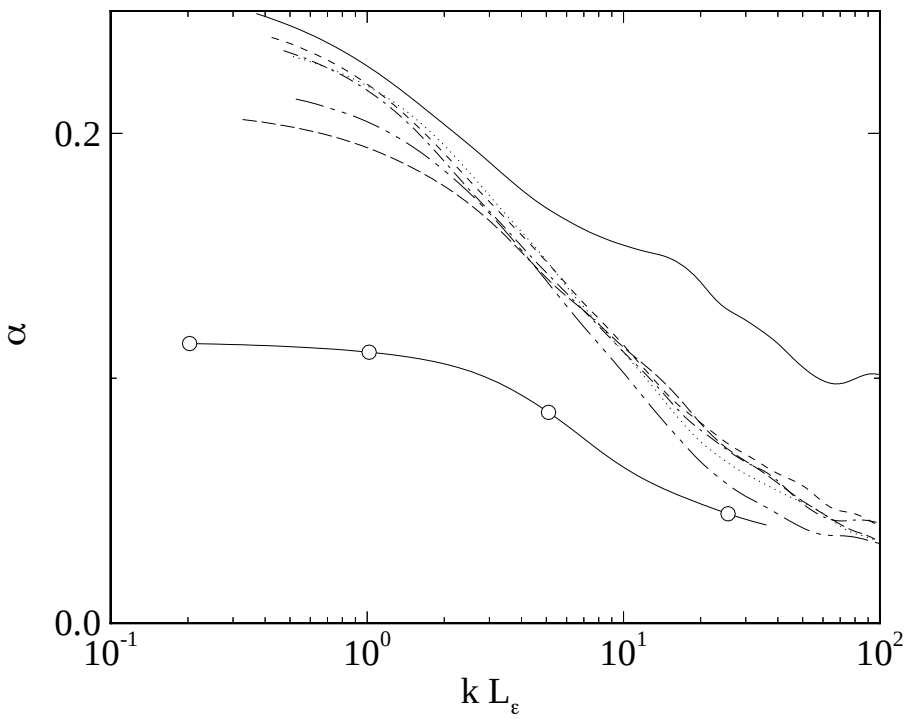


FIGURE 1. Root-mean square subgrid stress anisotropy as a function of the cut-off wavenumber for sharp Fourier filtering. Non-equilibrium boundary layer in an adverse pressure gradient (Marušić & Perry 1995): $Re_\tau = 1253$, $(\delta^*/\tau_w)\,\mathrm{d}P/\mathrm{d}x = 7.16$. ——— , $y/\delta = 0.049$; - - - - , 0.069; —·— , 0.095; ····· , 0.168; —··— , 0.328; — — — , 0.630. Circular jet from (Bradshaw, Ferris & Johnson 1964): —○— . $UR/\nu = 1.7 \times 10^5$, $x/R = 4$, $y/R = 1$.

The issues involved in this substitution are discussed by Batchelor (1953) for the particular case of isotropic turbulence where, within the inertial range, isotropy implies that $\Theta_{22} = \Theta_{33} = \frac{4}{3}\Theta_{11}$. In a more general case the substitution cannot be completely compensated. In the experiments discussed below, it has been taken approximately into account by premultiplying $\Theta_{11}$ by 4/3. Even so, the anisotropy becomes uncertain as it approaches the value $\alpha \approx 0.04$, which corresponds to a tensor whose principal stresses are in the ratio (1, 4/3, 4/3).

Two experimental flows are analyzed in this way in Fig. 1: a non-equilibrium boundary layer in a strong adverse pressure gradient (Marušić & Perry 1995), and a circular jet (Bradshaw, Ferris & Johnson 1964). Several wall distances are used in the boundary layer and, in all cases, the streamwise wavenumber is normalized with the integral dissipation length $L_\epsilon = q^3/\epsilon$, where $q^2 = \overline{u_i u_i}$, and $\epsilon$ is the energy dissipation rate. The integral dissipation length is always of the same order as the integral scales of the flow and is generally much easier to compute. It can be seen that, although the large scales are fairly different in both flows, they become essentially isotropic for $kL_\epsilon > 50$, corresponding to a filter of width $\Delta x = 2\pi/k \approx L_\epsilon/10$. The exception is the station of the boundary layer very close to the wall, $y^+ \approx 60$, which either does not reach isotropy or does it very slowly. The microscale Reynolds

number is comparable in both cases, $Re_\lambda \approx 150 - 200$, even in the neighborhood of the wall. The differences observed in the behavior of the near-wall spectrum are probably not due to low Reynolds number effects.

Perhaps more relevant to LES is the total, rather than relative, stress anisotropy. Figure 2(a) contains subgrid spectra of the total anisotropic stress, $\tau_A = \alpha^2 \tau_{ii}(k)$, while Fig. 2(b) displays spectra of the $\tau_{12}(k)$, which is the only off-diagonal stress which does not vanish identically in these experiments. All the spectra have been normalized to unity at $k = 0$ and give the fraction of the stresses that would have to be represented by a subgrid model.

The classical scale similarity theory for the cospectrum predicts $\Phi_{12} \sim k^{-7/3}$ (Lumley 1967 ), which would translate into $\tau_{12} \sim k^{-4/3}$ for the accumulated subgrid cospectrum. A line with this slope has been included in both Fig. 2(a) and (b), but it fits the data only approximately. As in the analysis of the previous figure, it follows from this one that $kL_\epsilon \approx 100$ marks the 'engineering' limit of anisotropic turbulence. The anisotropic subgrid stresses beyond that limit are less than 1% of the total, and even gross errors in their prediction would have a slight effect on the mean flow.

### *2.2 Triaxial filters*

The analysis in the previous section was restricted to one-dimensional filters by the experimental information at hand. A full study of the subgrid stresses under generic triaxial filtering requires knowledge of the full spectral tensor or, equivalently, of the full three-dimensional autocorrelation tensor of the velocities. Both tensors are related by a Fourier transform. The correlation tensor $R_{ij}(\mathbf{x}, \mathbf{x}') = \langle u_i(\mathbf{x}),\, u_j(\mathbf{x}') \rangle$, where $\langle\rangle$ stands for averaging, is a function of the two points $\mathbf{x}$ and $\mathbf{x}'$ and only becomes a function of the relative displacement $\mathbf{x} - \mathbf{x}'$ along the homogeneous directions of the flow. In the general case it is a six-dimensional object that is seldom compiled in experiments or computations.

If a filter is defined as a convolution

$$\overline{u} = \int g(x,\, x') u(x')\, \mathrm{d}x', \tag{2.5}$$

the exact filtered second-order statistics can be obtained from the correlation tensor by a double filtering operation (Jiménez & Moser 1997),

$$R_{\overline{u}\,\overline{v}}(x,\, x') = \int\int R_{uv}(\xi,\, \xi') g(x,\, \xi) g(x',\, \xi')\, \mathrm{d}\xi\, \mathrm{d}\xi'. \tag{2.6}$$

For $x = x'$, we recover the filtered one-point second order statistics $R_{\overline{u}\,\overline{v}}(x,\, x) = \langle \overline{u}\,\overline{v} \rangle$, and the subgrid stresses can be obtained by subtracting the filtered from the unfiltered values, $\tau_{uv} = R_{uv} - R_{\overline{u}\,\overline{v}}$. Besides being applicable to inhomogeneous flows, this procedure has the advantage of requiring only the small-separation correlation tensors (over separation distances less than or equal to the longest desired filter length), thus relaxing somewhat the storage and computational requirements of dealing with such high-dimensional objects.

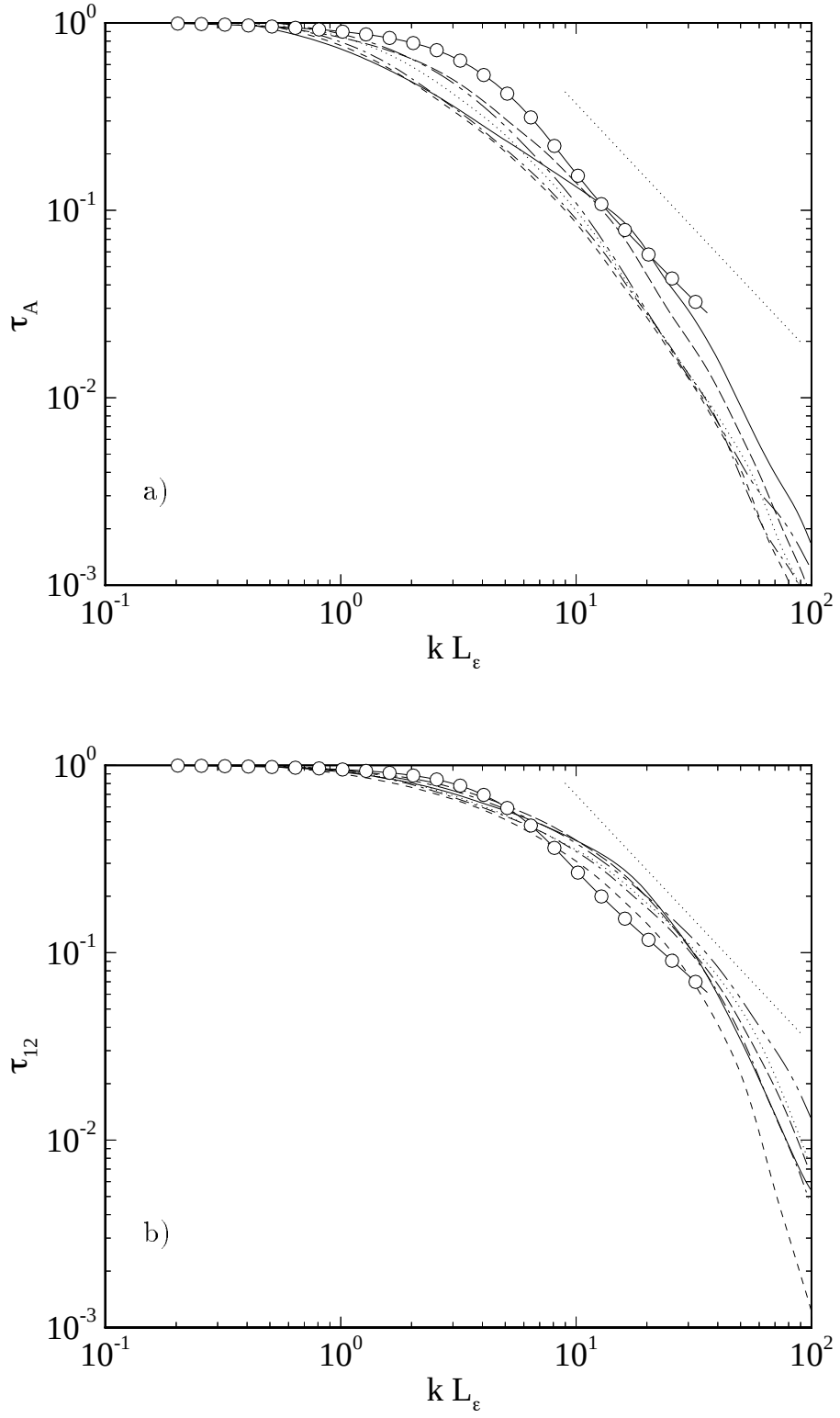


FIGURE 2. Subgrid stress spectra for the experiments in Fig. 1. (a) Total anisotropic stress. (b) Off-diagonal component, $\tau_{12}$. Symbols as in Fig. 1. The two dotted straight lines have spectral slope $k^{-4/3}$, as suggested by the inertial theory for the cospectrum.

A compilation of data intended for the validation of LES has recently become available (AGARD 1998), and contains correlation data for several flows. The boundary layer spectra used in the previous section also belong to this collection. Here we use data from a $Re_\tau = 590$ channel computed by Mansour, Moser & Kim (1997) to obtain scaling information for the subgrid stresses under anisotropic filters. The data are compiled at seven locations in the channel, $y^+ = 60 - 500$, and two types of filters are used: a simple box filter

$$g = (\delta_1 \delta_2 \delta_3)^{-1}, \qquad \text{for} \quad |x_i - x_i'| < \delta_i/2, \qquad i = 1 \ldots 3, \tag{2.7}$$

which vanishes for $|x_i - x_i'| > \delta_i/2$, and a Gaussian one adjusted so that its variance is the same as that of the box filter in each direction. Each of the $\delta_i$ are varied independently in the range from zero (actually the computational grid spacing of a few wall units) to $\delta_i \approx 0.14H$, where $H$ is the half-width of the channel. This generates approximately 700 filter combinations at each location, and the fractional subgrid stresses $\tau_{ij}/\langle u_i u_j \rangle$ are compiled in each case.

The equivalent width to be used for anisotropic filters was first considered by Deardorff (1970) and has been discussed since then by Schuman (1975), Lilly (1988), and Scotti, Meneveau & Fatica (1996). A popular choice is $\Delta = (\delta_1 \delta_2 \delta_3)^{1/3}$, which was first proposed by Deardorff and which can be approximately justified by considering the integrated dissipation in a Kolmogorov spectrum outside the wavenumber ellipsoid that represents the filter. That scale is, however, not necessarily relevant for the prediction of the subgrid stresses since their spectral tensor is very different from that of the dissipation, and the dominant contributions to the former are due to the anisotropic large scales rather than to the isotropic ones which dominate the latter. In fact, the subgrid stresses from the different filters collapse very poorly when plotted against isotropic combinations of the widths, as seen in Figs. 3A(a)-3B(a). Note that, although we have used in those figures a quadratic combination, the performance of the Deardorff criterion is actually poorer.

It turns out that the optimum collapse of each subgrid stress is obtained for a different combination of $\delta$'s. By adjusting the coefficients of the squares to obtain a minimum scatter we find, for example, that the best equivalent width for $\tau_{11}$ is (Fig. 3A(b))

$$\Delta_{11} = (\delta_1^2 + 2\delta_2^2 + 2\delta_3^2)^{1/2}. \tag{2.8}$$

This is easily understood by assuming that turbulence is approximately isotropic, even in this shear flow. For small separations we can approximate the correlation function by

$$R_{11}/\langle u_1 u_1 \rangle = 1 - \sum \frac{(x_i' - x_i)^2}{2\lambda_{11,i}^2} + \ldots, \tag{2.9}$$

and it follows from isotropy that the longitudinal and transverse Taylor microscales are related by (Batchelor 1953)

$$\lambda_{11,1}^2 = 2\lambda_{11,2}^2 = 2\lambda_{11,3}^2. \tag{2.10}$$

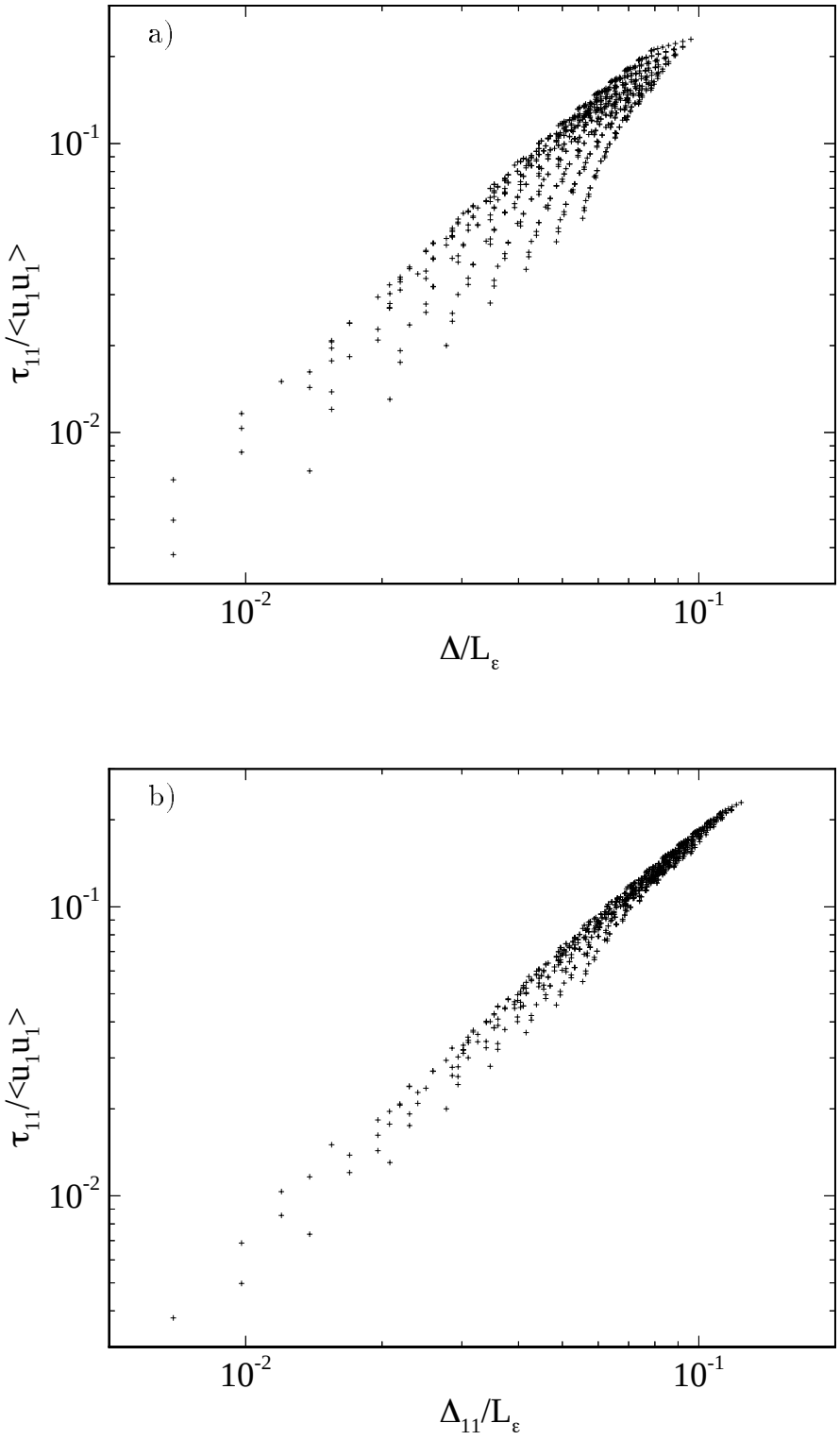


FIGURE 3A. Subgrid stresses in a channel flow (Mansour, Moser & Kim 1997) using triaxial filters: $\tau_{11}$ component. + , box filter. Figure (a) uses $\Delta = (\delta_1^2+\delta_2^2+\delta_3^2)$ in the abscissa. Figure (b) uses $\Delta_{11}$ given by (2.8). $Re_\tau = 590$, $y^+ = 300$.

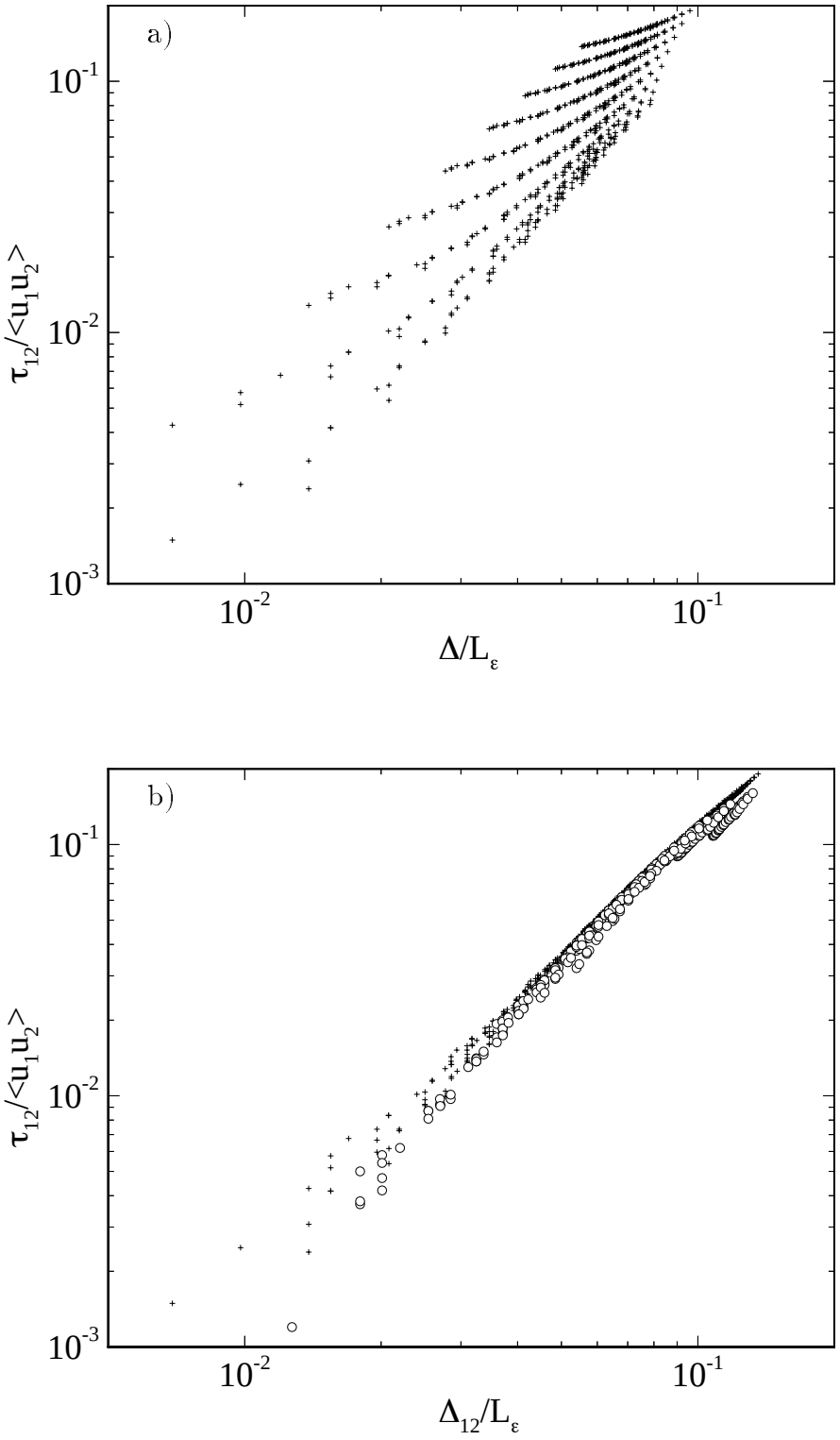


FIGURE 3B. Subgrid stresses in a channel flow (Mansour, Moser & Kim 1997) using triaxial filters: $\tau_{12}$ component. + , box filter; ∘ , Gaussian. Figure (a) uses $\Delta = (\delta_1^2 + \delta_2^2 + \delta_3^2)$ in the abscissa. Figure (b) uses $\Delta_{12}$ given by (2.13). $Re_\tau = 590$, $y^+ = 300$.

If we remember that the filtered stresses are essentially the integral of (2.9) within a box defined by the filter, it is reasonable to expect that the relevant scale combination should weigh the different widths with the curvatures of the function along each axis. This, together with (2.10), leads to (2.8). Applying the same argument to $R_{22}$ and $R_{33}$ suggests that the right combinations for $\tau_{22}$ and $\tau_{33}$ should be

$$\Delta_{22} = (2\delta_1^2 + \delta_2^2 + 2\delta_2^2)^{1/2}, \tag{2.11}$$

$$\Delta_{33} = (2\delta_1^2 + 2\delta_2^2 + \delta_3^2)^{1/2}. \tag{2.12}$$

Although they are not shown in the figure, these predictions turn out to be correct.

The isotropic theory does not give information on the scaling of the off-diagonal stresses, which vanish identically in that case. The empirical optimum combination for the present channel is very close to (Fig. 3B(b))

$$\Delta_{12} = (\delta_1^2 + \delta_2^2 + 4\delta_3^2)^{1/2}, \tag{2.13}$$

which is simple enough to suggest that a theoretical explanation should exist, probably as a perturbation of the isotropic theory including weak shear. Also in this case it is easy to check that the scaling factors correspond to the curvatures of the correlation function in the neighborhood of the origin. It is clear, on the other hand, that these scalings can only be approximations, valid for a particular range of filter scales which are comparable to the Taylor microscale. Much wider filters act on regions of the correlation functions which are not well described by the parabolic approximation (2.9), and they should not scale well with the Taylor microscales. Also, other flows are intrinsically anisotropic, and the isotropic approximation that holds here would not apply to them. Some preliminary tests on homogeneous shear flows (Rogers & Moin 1987, Sarkar 1995) suggest that, although simple quadratic combinations also work well for them, they are different from the ones above. Note that the results of the Gaussian filters have been included in Fig. 3B(b), and that they approximately agree with those of the box filters.

The use of the integral dissipation length to scale the equivalent filters works well here as it did for the spectra in the previous section. In Fig. 4 we have compiled data from several locations in the channel, among which the integral dissipation length varies by up to a factor of two and the collapse of $\tau_{12}$ is maintained.

## 3. Simulations

To compare the subgrid stresses predicted above with those actually provided by standard LES models, we undertook a set of simulations of a plane channel at $Re_\tau \approx 1,000$. They use a multiblock code which allows a high resolution to be maintained near the walls while varying the grid in the center of the channel. This avoids the issues of the representation of the flow near the wall, which are known to be important, while permitting a systematic survey of the effect of the resolution in the central part of the flow. The code itself and its performance across block boundaries are described by Kravchenko, Moin & Moser (1996). It uses a

double Fourier expansion in the periodic streamwise and spanwise directions, and second-order splines normal to the wall. Three computations are analyzed here, all of them using a box of size $2\pi \times 2 \times \pi/2$. The spanwise dimension is narrow for an accurate representation of the central core region, but it should be wide enough for the logarithmic range below $y^+ \approx 500$. The three simulations are comparable to each other except for the resolution. They all use standard dynamic Smagorinsky subgrid modeling with the proportionality constant averaged over planes parallel to the walls.

The first simulation uses a single-block grid $48 \times 64 \times 48$ in the streamwise, normal, and spanwise dimensions. It was checked against a previous simulation on a somewhat larger box ($2\pi \times 2 \times \pi$) at higher resolution, $96 \times 100 \times 96$, and it is considered to be approximately correct. The two other simulations use the same grid near the walls ($48 \times 21 \times 48$), but the horizontal resolution is decreased in a central block, which contains 22 points for the region above $y^+ \approx 250$. The horizontal grids in this region are $24 \times 24$, and $16 \times 16$. The horizontal resolution of the finer grid is $\Delta x^+ \times \Delta z^+ \approx 130 \times 30$ and becomes respectively two and three times coarser for the other two grids. The wall-normal resolution is identical in all cases and varies from $\Delta y^+ \approx 0.5$ near the wall to $\Delta y^+ \approx 100$ at the center of the channel.

In each case the fraction of the mean subgrid shear stress $\tau_{12}$ due to the model was recorded as a function of $y$. It is given in Fig. 4 in terms of a reduced 'filter' size computed from the local grid spacing using (2.13) and normalized with the local integral dissipation length. Only points in the central block and at least two grid points away from the zonal boundaries are used. Included for comparison are the subgrid fractions of the same quantity obtained in the previous section (Fig. 3d) by explicit filtering of the direct channel simulation.

It is remarkable that both sets of data collapse reasonably well within themselves, taking into account that they represent filters of widely varying aspect ratios at locations in the channel that span from the inner logarithmic region to the central core. They do not, however, agree with each other. The measured subgrid stresses are consistently below those predicted by explicit filtering, by a factor of about 3–4.

Note that the two sets are not strictly comparable since the filtering results are plotted against a known filter width, while the filter width in the simulation is assumed proportional to the grid size with the grid acting as an unknown implicit filter. They should therefore not be expected to agree exactly with each other, but the disagreement is in the wrong direction. Even if the effect of the grid is not well understood, it is clear that it cannot represent features smaller than the grid spacing. This implies that the stresses in the subgrid eddies should correspond to filters at least as wide as the grid, and probably wider, while the only way to collapse the two sets of data in the figure would be to assume that the grid is acting as a filter three times narrower than itself. The only possible conclusion is that the subgrid model is providing at most about 20–30% of the shear stress that it should, in rough agreement with the results obtained by Bardina *et al.* (1983) from *a-priori* testing of the Smagorinsky model.

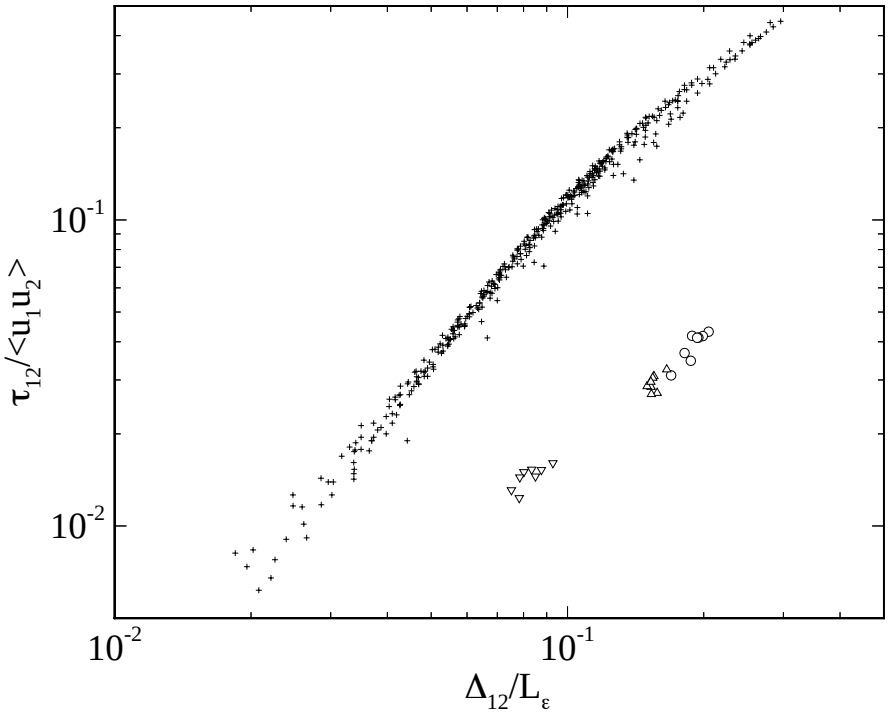


FIGURE 4. Fraction of the subgrid shear stress carried by the dynamic Smagorinsky model, compared with what should be carried at a comparable filtering size. LES simulations of channel at $Re_\tau \approx 1000$, $y^+ > 300$. Resolution in central block: $\circ$ , $16 \times 16$; $\triangle$ , $24 \times 24$; $\nabla$ : $48 \times 48$. Resolution near the wall is always $48 \times 48$. $+$ , subgrid $\tau_{12}$ obtained by explicit box filtering on a channel at $Re_\tau = 590$, as in Fig. 3. $y^+ > 90$.

It follows that, if the shear stress is underrepresented by the model, the velocity profile should adjust itself until the total stress is that of an equilibrium channel, which varies linearly between the two walls. The errors in the mean velocity profile should then become worse as the resolution is made coarser, making the model responsible for a larger fraction of the total stresses. This can be seen to be true in Fig. 5, which shows the Kármán constant computed from each simulation. It agrees reasonably well with the accepted experimental value $\kappa \approx 0.4$, in the finer grid, where the subgrid stress should be in the range of 5–8% (Fig. 4). Even if in this case the modeled stresses are only about 1%, the total error is 5%, and the effect on the mean flow is slight. In the coarser simulation, it follows from the figure that the subgrid stresses should be of the order of 20%, while those provided by the model are only about 5%. The resulting 15% error translates into an error of the same order of magnitude in the Kármán constant and in the mean profile.

## 4. Discussion and conclusions

### *4.1 Degrees of freedom*

The analysis in the previous sections suggests that accurate subgrid models for

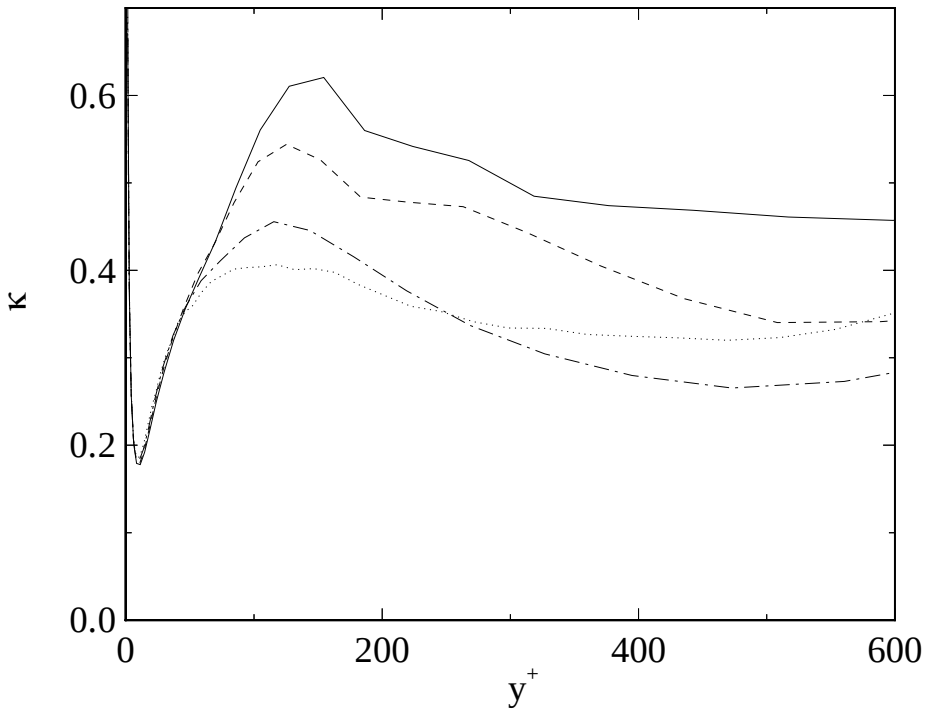


FIGURE 5. Kármán constant, $\kappa = (y\partial U^+/\partial y)^{-1}$, computed from the large-eddy simulations in Fig. 4. Resolution in central block: ——— , $16 \times 16$; - - - - , $24 \times 24$; —·— , $48 \times 48$. ····· , single-block computation on a $96 \times 100 \times 96$ grid, in a larger box, $2\pi \times 2 \times \pi$; included for comparison.

the Reynolds stresses, which are large-scale properties of the flow, may not be strictly necessary in all practical LES. They can be avoided by refining the LES filter until the fraction of the stresses to be modeled becomes negligible, and this happens at a fixed fraction of the integral dissipation length, $\Delta x \approx L_\epsilon/10$. Besides the evidence from the experiments analyzed above, this is a consequence of the form of the spectra of the subgrid stresses, which decay approximately as $k^{-2/3}$ for the isotropic components and as $k^{-4/3}$ for the anisotropic ones. The integral scale is defined by the peak of the energy spectrum, and the decay of the stresses is therefore measured with respect to it. In the cases in which turbulence is driven by large-scale shear, the energy-containing eddies are controlled by the geometry, and the previous argument shows that modeling the stresses correctly requires filters which are a fixed fraction of the geometric scale. This implies that, for situations in which $L_\epsilon$ is approximately uniform, as in free shear flows, only a few thousand degrees of freedom need to be computed explicitly, independently of the Reynolds number. All the stresses are contained essentially in them.

Note that the last part of this argument may not be valid if the turbulent forcing is due to factors other than the geometry, in which case the integral scales can be smaller than the geometric ones and may depend on the Reynolds number. Such may be the case, for example, in two phase flows and in turbulent natural convection.

The situation is different for the rate of energy dissipation, which is associated

with eddies of the order of the Kolmogorov scale $\eta \sim L_\epsilon Re^{-3/4}$ and which has to be estimated correctly to avoid the accumulation of energy in the small scales (Jiménez 1993, 1995). In the absence of good subgrid models for the dissipation, this would require the computation of all the eddies down to the level of $\eta$ and would lead to the well known estimate of the number of degrees of freedom in direct simulations, $N_T \sim Re^{9/4}$. What the previous analysis suggests is that modeling the dissipation and the stresses are different tasks, with different requirements, and could possibly be handled by different models. It also shows that, while modeling the former is an absolute requirement for practical simulations, modeling the latter may not be crucial.

The previous arguments do not apply in the neighborhood of a wall. While the data discussed above shows that the anisotropic modes are confined to eddies larger than a given fraction of the integral scales even in the logarithmic wall layer, the integral scales decrease as we approach the wall. Consider a fluid volume whose size $L_{\epsilon 0}^3$ is determined by the geometric scales, such as the channel half-width. In the neighborhood of the wall the integral length decreases linearly as $L_\epsilon \sim y$, and the eddies remain anisotropic above $\Delta x \sim y$. The number of anisotropic modes in a slab of thickness $\mathrm{d}y$ is then $\mathrm{d}N \sim L_{\epsilon 0}^2 \,\mathrm{d}y/\Delta x^3$, and their total number is given by the integral

$$N_T \sim \int_{y_0}^{\infty} L_{\epsilon 0}^2 \,\mathrm{d}y/y^3 \sim L_{\epsilon 0}^2/y_0^2, \tag{4.1}$$

where $y_0$ is some inner wall distance that determines the number of modes. If, in the absence of a good model for anisotropic turbulence, we choose this limit as a fixed number of viscous wall units, $y_0 = \nu y_0^+/u_\tau$, the number of anisotropic modes becomes

$$N_T \sim (u_\tau L_{\epsilon 0}/\nu)^2 = Re_\tau^2, \tag{4.2}$$

which is only slightly lower than the estimation for direct numerical simulation and which increases without limit with the Reynolds number. Note that this estimation is not linked to a particular numerical model, being just a count of the number of 'non-Kolmogorov' modes per unit volume of wall turbulence. These modes depend on more parameters than the rate of energy dissipation, and they are unlikely to be modeled correctly by isotropic approximations of the Smagorinsky type.

Note also that improving the subgrid models so that they represent a higher fraction of the stresses, so that the filter can be chosen as a higher fraction of the integral scale, would only modify the numerical coefficient in (4.2), but not its Reynolds number dependence. The only alternatives to decrease substantially the explicitly computed number of modes would be to improve the subgrid models to represent correctly *all* the Reynolds stresses, even above the integral scale, or to stop the computation at some distance $y_0$ from the wall, expressed in outer, rather than wall, units.

### *4.2 Conclusions and future work*

We have shown that the anisotropic subgrid stresses are confined in practice to eddies larger than about one tenth of the local integral dissipation scale, and we have

given criteria to compute the equivalent width, for this purpose, of triaxial filters in weakly sheared, quasi-equilibrium, flows. We have also shown that Smagorinsky-type dynamic subgrid models, while representing the energy dissipation correctly, are not able to reproduce the stresses. They only work if the filter widths are chosen so that the subgrid stresses to be modeled are a negligible fraction of the total. The errors due to the model then become unimportant.

For free shear flows this results in a number of degrees of freedom that have to be computed explicitly, which is independent of the Reynolds number, of the order of a few thousands. This would make LES a practical alternative in many applications.

For wall bounded flows the same criterion results in a number of anisotropic, 'non-Kolmogorov', modes which scales like $Re_\tau^2$, most of which are concentrated near the wall. To avoid this Reynolds number dependence, the two alternatives are either to develop better models which are able to describe correctly the full shear stresses, or to find wall representations which can be applied at distances which do not scale in wall units.

Some preliminary tests of mixed Bardina-type models (Vreman, Geurts & Kuerten 1994) disappointingly gave worse results than the Dynamic Smagorinsky model at comparable resolutions, but more work is needed before that line is abandoned. The conclusions of the present work also need to be extended to more general non-equilibrium flows.

## Acknowledgments

We have benefitted from fruitful discussions with W. Cabot, J. Ferziger and P. Moin. The work was supported in part by AFOSR grant #F49620-97-1-0210. Special thanks are due to W. Cabot for reviewing the preliminary version of this manuscript.

## REFERENCES

AGARD 1998 A selection of test cases for the validation of large-eddy simulations of turbulent flows. *AR-345.*

Bardina, J., Ferziger, J. H. & Reynolds, W. C. 1983 Improved turbulence models based on large-eddy simulation of homogeneous, incompressible, turbulent flows. *Thermosciences Div. Rep.* **TF-19,** Stanford Univ.

Batchelor, G. K. 1953 *The theory of homogeneous turbulence.* Cambridge Univ. Press.

Bradshaw, P., Ferris, D. H. & Johnson, R. H. 1964 Turbulence in the noise-producing region of a circular jet. *J. Fluid Mech.* **19,** 591-624.

Chapman, D. R. 1979 Computational aerodynamics development and outlook. *AIAA J.* **17,** 1293-1313.

Clark, R. A., Ferziger, J. H. & Reynolds, W.C. 1979 Evaluation of subgrid-scale models using an accurately simulated turbulent flow. *J. Fluid Mech.* **91,** 1-16.

DEARDORFF, W. 1970 A numerical study of three-dimensional turbulent channel flow at large Reynolds numbers. *J. Fluid Mech.* **41,** 453-480.

GERMANO, M., PIOMELLI, U., MOIN, P. & CABOT, W. H. 1991 A dynamic subgrid scale eddy viscosity model. *Phys. Fluids.* **A**(3)**,** 1760-1765. Erratum, *Phys. Fluids* A **3**, 3128.

JIMÉNEZ, J. 1993 Energy transfer and constrained simulations in isotropic turbulence. *CTR Res. Briefs,* Center for Turbulence Research, NASA Ames/Stanford Univ., 171-186.

JIMÉNEZ, J. 1995 On why dynamic subgrid-scale models work. *CTR Res. Briefs,* Center for Turbulence Research, NASA Ames/Stanford Univ., 25-34.

JIMÉNEZ, J. & MOSER, R.D. 1997 Data filtering and file formats, §2 of. *AGARD.* **AR-345,** 5-8.

KOLMOGOROV, A. N. 1941 The local structure of turbulence in incompressible viscous fluids a very large Reynolds numbers. *Dokl. Nauk. SSSR.* **30,** 301-305 (see e.g. L. D. Landau & E. M. Lifshitz, 1959, *Fluid mechanics*, Pergamon, 116-123).

KRAVCHENKO, A. G., MOIN, P. & MOSER, R. D. 1996 Zonal embedded grids for numerical simulations of wall-bounded turbulent flows. *J. Comp. Phys.* **127,** 412-423.

LILLY,D. 1988 The length scale for sub-grid-scale parameterization with anisotropic resolution. *CTR Res. Briefs,* Center for Turbulence Research, NASA Ames/Stanford Univ., 3-9.

LUMLEY, J. L. 1967 Similarity and turbulent energy spectrum. *Phys. Fluids.* **10,** 855-858.

MANSOUR, N. N., MOSER, R. D. & KIM, J. 1996 Reynolds number effects in low Reynolds number turbulent channels. *In preparation.*

MARUŠIĆ, I. & PERRY, A. E. 1995 A wall-wake model for the turbulence structure of boundary layers. Part 2. Further experimental support. *J. Fluid Mech.* **298,** 389-407. Case TBL10 in AGARD (1997).

MOIN, P. 1997 Progress in large eddy simulation of turbulent flows. *AIAA Paper.* **97-0749.**

MOIN, P. & JIMÉNEZ, J. 1993 Large eddy simulation of complex turbulent flows. *AIAA Paper.* **93-3099.**

ROGERS, M. M. & MOIN, P. 1987 The structure of the vorticity field in homogeneous turbulent flows. *J. Fluid Mech.* **176,** 33-66.

SARKAR, S. 1995 The stabilizing effect of compressibility in turbulent shear flow. *J. Fluid Mech.* **282,** 163-186.

SADDOUGHI, S. G. & VEERAVALLI, S. V. 1994 Local isotropy in turbulent boundary layers at high Reynolds number. *J. Fluid Mech.* **268,** 333-372.

SCHUMANN, U. 1975 Subgrid-scale model for the finite-difference simulations of turbulent flows in plane channels and annuli. *J. Comput. Phys.* **18,** 376-404.

SCOTTI, A., MENEVEAU, C. & FATICA, M. 1996 Dynamic Smagorinsky model on anisotropic grids. *Proceedings CTR 1996 Summer Program,* Center for Turbulence Research, NASA Ames/Stanford Univ., 259-274.

VREMAN, B., GEURTS, B. & KUERTEN, H. 1994 On the formulation of the dynamic mixed subgrid-scale model. *Phys. Fluids.* **6,** 4057-4059.